

One-particle and excitonic band structure in cubic Boron Arsenide

Swagata Acharya,^{1,2} Dimitar Pashov,³ Mikhail I Katsnelson,² and Mark van Schilfgaarde^{1,3}

¹*National Renewable Energy Laboratories, Golden, CO 80401, USA*

²*Institute for Molecules and Materials, Radboud University, NL-6525 AJ Nijmegen, The Netherlands**

³*King's College London, Theory and Simulation of Condensed Matter, The Strand, WC2R 2LS London, UK*

Cubic BAs has received recent attention for its large electron and hole mobilities and large thermal conductivity. This is a rare and much desired combination in semiconductor industry: commercial semiconductors typically have high electron mobilities, or hole mobilities, or large thermal conductivities, but not all of them together. Here we report predictions from an advanced self-consistent many body perturbative theory and show that with respect to one-particle properties, BAs is strikingly similar to Si. There are some important differences, notably there is an unusually small variation in the valence band masses. With respect to two-particle properties, significant differences with Si appear. We report the excitonic spectrum for both $\mathbf{q}=0$ and finite \mathbf{q} , and show that while the direct gap in cubic BAs is about 4eV, dark excitons can be observed down to about ~ 1.5 eV, which may play a crucial role in application of BAs in optoelectronics.

I. INTRODUCTION

Zincblende BAs has received considerable attention recently¹ because of its large ambipolar mobility and large thermal conductivities. It is a rare yet much desired combination. Silicon — the foundation for much of modern day technology — has poor hole mobility and also is a bad thermal conductor and, hence, suffers from overheating issues. BAs has thermal conductivity that is nearly ten times higher than silicon and nearly half of that of diamond. A series of theoretical² and experimental works³⁻⁵ almost unambiguously established these facts. However, experimental determination of the ambipolar mobilities have been more difficult to establish. A density-functional calculation in 2018⁶ predicted high electron and hole mobilities of $\mu_e=1400$ cm² V⁻¹ s⁻¹ and $\mu_h=2100$ cm² V⁻¹ s⁻¹. However, a subsequent experimental work found the hole mobility to be as low as 22 cm² V⁻¹ s⁻¹. Defects were thought to be the key factor limiting the hole mobility and it demanded an experimental approach where thermal and electrical conductivities could be measured for the intrinsic sample without being defect-limited. Shin et al.¹ achieved this goal by employing transient grating method that simultaneously measured thermal (κ_{RT}) and electrical conductivities (or, equivalently, μ_e, μ_h) at different spots (and a small region around them) of the sample which are free from defects and provide the information of the intrinsic mobilities. With that they found $\mu_h > 1000$ cm² V⁻¹ s⁻¹, ambipolar mobility $2\mu_e\mu_h/(\mu_e + \mu_h)$ of 1600 cm² V⁻¹ s⁻¹ and κ_{RT} of 1200 Wm⁻¹K⁻¹. Recent works by Yue et al.⁷ and Choudhry et al.⁸ also establish these facts from transient reflectivity microscopy and ultrafast electron microscopy, respectively. These observations make cubic BAs an attractive candidate for next generation semiconductor based technologies.

II. RESULTS AND DISCUSSION

A. Electronic properties

1. Electronic band gap

However, still there exists some ambiguities related to its electronic band gap, the anisotropies of the hole and electron mass tensors, dielectric constant and excitonic properties. Several experimental and theoretical works have reported significantly different numbers for these properties (see Table 1 in the work by Buckeridge and Scanlon⁹). The calculations from Buckeridge and Scanlon are performed on a zinc-blende structure of BAs. Buckeridge and Scanlon reports an indirect band gap of 1.67 eV from their calculations. Older experimental studies report band gap of ~ 1.5 eV,¹⁰⁻¹² though a more recent measurement reports a gap of 1.82 eV,¹³ and another 2.02 eV from high-quality millimeter-sized crystals.¹⁴ A single shot G_0W_0 calculation performed with BerkleyGW yielded a gap of 2.07 eV and another work reports a gap of 1.78 eV.¹⁵ Here we use quasiparticle self-consistent GW theory (QSGW),^{16,17} which, in contrast to conventional GW methods, modifies the charge density and is determined by a variational principle,¹⁸ and QSGW¹⁹ in which the screened coulomb interaction W is computed including vertex corrections (ladder diagrams) by solving a Bethe-Salpeter equation (BSE) within Tamm-Dancoff approximation.²⁰ Crucially, QSGW and QSGW¹⁹ are fully self-consistent in both self-energy Σ and the charge density.²¹ G , Σ , and \widehat{W} are updated iteratively until all of them converge. Zincblende semiconductors are described with uniformly high fidelity in QSGW,¹⁹ and we can expect similar agreement for BAs. We find the electronic indirect band gap to be 2.00 eV within QSGW and 1.85 eV within QSGW¹⁹, indicating that vertex corrections to the GW self-energy are modest, as is typically found in III-V semiconductors. (Since QSGW¹⁹ systematically underestimates the Γ -X transition

by 0.1 to 0.15 eV in zincblende semiconductors¹⁹ the true bandgap is probably closer to 2.0 eV).

TABLE I. Conduction band properties of BAs, at different levels of the theory: bandgaps, effective masses and non-parabolicity parameter α . Si results are shown for comparison. Experimental masses are taken from Ref. 22; the direct gap from Ref. 23.

Theory	E_G	$E_G(\text{dir})$	m_{\parallel}	m_{\perp}	α_{\perp}
LDA	1.07	3.04	1.23	0.26	-7.1
QSGW	2.00	4.26	0.96	0.25	-7.0
QSGW	1.85	4.08	1.03	0.25	-7.4
QSGW, Si	1.22	3.23	0.92	0.19	0.2
Expt, Si	1.17	3.35	0.91	0.19	

TABLE II. QSGW Luttinger parameters for the valence band of BAs, compared to similar zincblende semiconductors.

	E_G	QSGW			Expt		
		γ_1	γ_2	γ_3	γ_1	γ_2	γ_3
Si ^a	1.13	4.24	0.32	1.42	4.26-4.29	0.34-0.38	1.45-1.56
AlAs ^b	2.14	3.99	0.89	1.45	3.42-3.44	0.67-1.23	1.17-1.57
GaAs ^b	1.63	6.75	1.83	2.74	6.79-7.20	1.90-2.88	2.68-3.05
BAs	1.85	4.33	0.05	1.29			

^a compilation in Ref. 24

^b compilation in Ref. 25

2. Electron and hole masses

A main focus of this work are the electron and hole masses. We compute the electron masses at the conduction band bottom near X, on the Γ -X line see Fig. 1, and the Luttinger parameters calculated from masses at the valence band maximum as

$$\begin{aligned}
 \gamma_1 &= \frac{1}{2m_{\text{hh}}^{001}} + \frac{1}{2m_{\text{hh}}^{001}} \\
 \gamma_2 &= \frac{1}{4m_{\text{hh}}^{001}} - \frac{1}{4m_{\text{hh}}^{001}} \\
 \gamma_3 &= \frac{1}{4m_{\text{hh}}^{001}} + \frac{1}{4m_{\text{hh}}^{001}} - \frac{1}{2m_{\text{hh}}^{111}}
 \end{aligned} \tag{1}$$

Our BSE electron masses are very similar to those of Buckeridge and Scanlon.⁹ Also, it is notable that higher levels of the theory only weakly modify the electron masses (see Table I). Also shown is the nonparabolicity parameter, defined as $m(E) = m^*(1 - \alpha E)$ (energy-dependent mass, with m^* the mass at $k=0$).

The split-off hole masses follow a pattern typical of zincblende semiconductors, with the former being essentially isotropic ($m^* \approx 0.24$) and $m_{\text{hh}}^{111} > m_{\text{hh}}^{110} > m_{\text{hh}}^{100}$, but the anisotropy is rather small (see γ_3 , Table II). Also notable is the smallness of γ_2 , so that along the 100 direction all three masses are nearly the same. This is

unusual, and is probably a consequence of the large direct gap at Γ . According to QSGW, the splitting of the split-off band is 220 meV, larger than Si (50 meV) and slightly smaller than smaller than AlAs (300 meV) and GaAs (340 meV).

The energy structure of BAs is quite similar to Si, both with the conduction band minimum on the Γ -X line near X. Both Si and BAs pick up significant d character near the conduction band minimum. The masses in the two materials are similar (Tables I and II). BAs is more polar than AlAs or GaAs: bands near the Fermi level are heavily weighted to the anion in BAs: bands of B character are mostly far above E_F .

B. Optical properties

We turn to the both macroscopic dielectric response and its \mathbf{q} -dependence within the BSE. We observe bright optical transitions at 4.0 eV (Bai-Song et al.¹⁴ reports 4.12 eV from their optical measurements), however, we find dark optical transitions down to ~ 1.5 eV. The deepest one is at the conduction band minimum along the Γ -X path. These transitions are dipole forbidden and completely dark in a purely electronic framework. We show the excitonic band structure in Fig. 2. Symmetry lowering mechanisms, such as defects, spin-orbit coupling, odd-parity phonon modes, Jan-Teller distortions can add to the oscillator strength of these otherwise dark excitons. We also note the nontrivial role that spin-orbit coupling (SOC) plays in reducing the electronic and optical band gaps. We find that SOC reduces the electronic band gap by ~ 90 meV and the optical gap by ~ 220 meV. However, the oscillator strengths of the deepest lying dark exciton only gets weakly enhanced in presence of SOC. To put it in perspective, in a purely electronic framework, without considering the impact phonons and defects can have on these excitons, the oscillator strength of the 1.5 eV peak remains at least three orders of magnitude lower than the 1.2 eV exciton in CrI_3 ^{26,27} and one order lower than the 1.6 eV exciton in NiO ²⁸ and at least eight orders lower than the exciton in monolayer of MoS_2 .²⁶ Interestingly enough, Shin et al.¹ observes a clear photo-luminescence peak at 695 nm (1.78 eV) in BAs. This is consistent with our observation that there exists a rich spectrum of excitonic eigenvalues deep inside the visible part of the optical spectrum, all the way down to the infrared edge. In particular, we observe a finite \mathbf{q} (Γ -X) excitonic transition at 1.75 eV. However, all such excitons are essentially of Wannier-Mott character as the electrons and holes that for these excitons come from essentially the conduction band bottom and valence band top.¹⁵ We also could not find any mention of such excitonic peaks in the combined experimental and theoretical optical studies from Bai-Song et al.¹⁴ We show in Fig. 2 the lowest conduction band in blue. The deepest lying excitonic band closely follows the conduction band profile. Along the entire path LFX the excitons remain

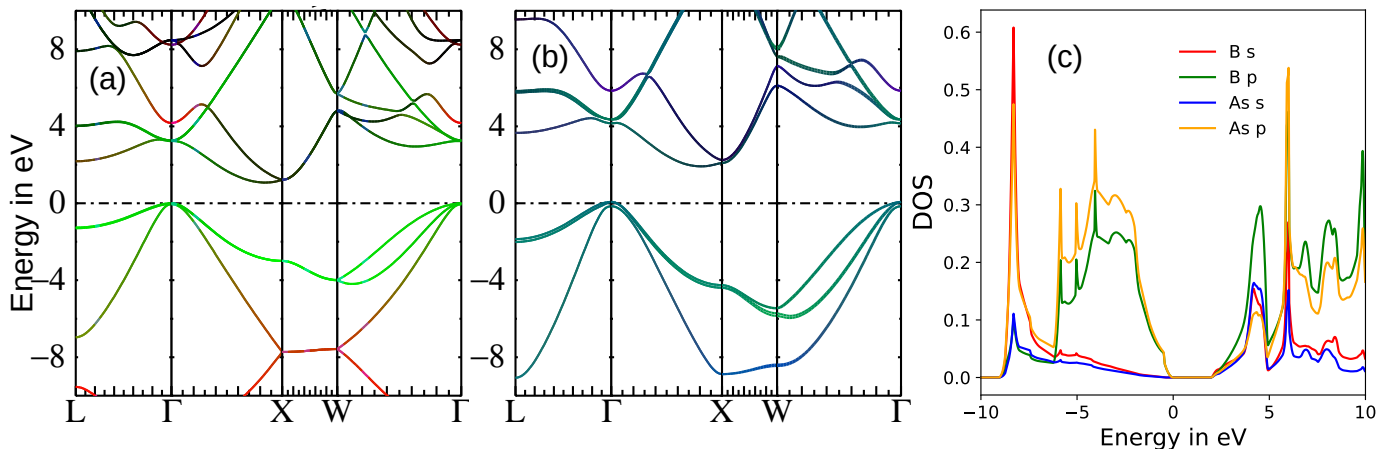


FIG. 1. **Energy bands:** QSGW energy bands compared to Si. (a) Si energy bands with green signify Si p character, red Si s character. (b) BAs bands with green signifying As p , red As s , and blue B $s+p$ characters. (c) The orbitaly projected density of states in BAs.

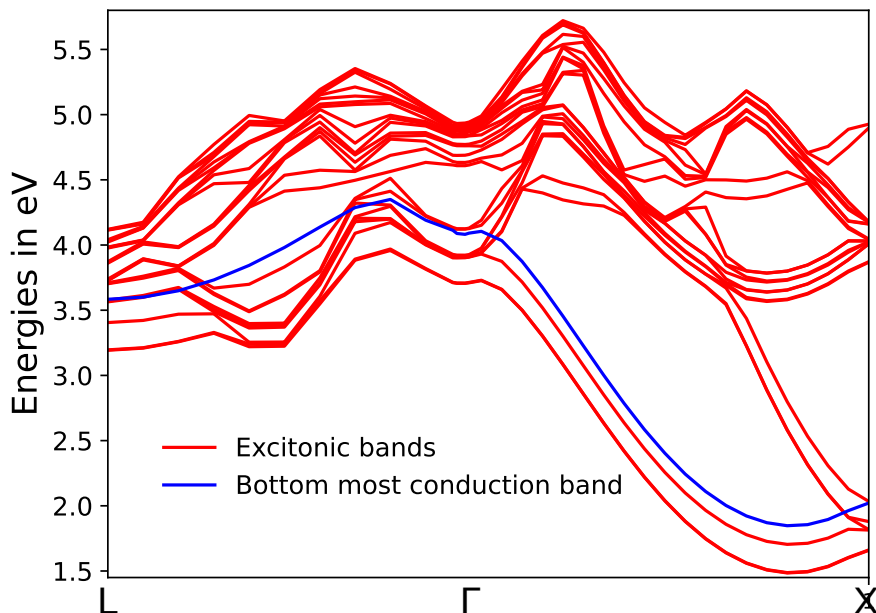


FIG. 2. **Excitonic band structure:** Exciton bands are shown along L Γ X path. The lowest conduction band is also shown. The deepest lying excitonic bands closely follow the conduction band profile. For excitons, the L, X and Γ signify the length of the \mathbf{q} vectors that connect the electrons to the holes and form excitons.

bound by roughly $\sim 0.2-0.3$ eV. Finally, within our approach we find the dielectric constant ϵ_∞ to be 8.75, while in the theoretical literature we find numbers between 8 and 9 (see Table. 1 from Buckeridge and Scanlon⁹). We also note that as the e-h vertex screens the RPA W , ϵ_∞ enhances from 6.55 to 8.75.

III. CONCLUSIONS

Altogether, these observations suggest that our calculated one- and two-particle properties are in all likelihood the correct intrinsic properties of cubic BAs. Our ob-

served electronic properties are in good agreement with experimental observations wherever data from defect-free cubic BAs is available. Further, we predict light hole masses and Luttinger parameters in BAs which might be significant considering the role BAs can play in semiconductor based devising. Finally we observe a very rich series of dark excitonic lines deep inside the visible part of the optical spectrum which can play a crucial role in application of cubic BAs in optoelectronics.

Supporting Information

We provide all input and output data files and commandlines to launch calculations that reproduce the re-

sults and figures from the paper at the deposition with digital object identifier.²⁹

Acknowledgements

MIK and SA are supported by the ERC Synergy Grant, project 854843 FASTCORR (Ultrafast dynamics of correlated electrons in solids). MvS (and SA in the late stages of this work) were supported the by the Computational Chemical Sciences program within the Office of Basic Energy Sciences, U.S. Department of Energy under

Contract No. DE- AC36-08GO28308. We acknowledge PRACE for awarding us access to Irene-Rome hosted by TGCC, France and Juwels Booster and Cluster, Germany. Late stages of calculations were performed using computational resources sponsored by the Department of Energy: the Eagle facility at NREL, sponsored by the Office of Energy Efficiency and also the National Energy Research Scientific Computing Center, under Contract No. DE-AC02-05CH11231 using NERSC award BES-ERCAP0021783.

-
- * swagata.acharya@nrel.gov
- ¹ J. Shin, G. A. Gamage, Z. Ding, K. Chen, F. Tian, X. Qian, J. Zhou, H. Lee, J. Zhou, L. Shi, *et al.*, *Science* **377**, 437 (2022).
 - ² L. Lindsay, D. Broido, and T. Reinecke, *Physical review letters* **111**, 025901 (2013).
 - ³ J. S. Kang, M. Li, H. Wu, H. Nguyen, and Y. Hu, *Science* **361**, 575 (2018).
 - ⁴ S. Li, Q. Zheng, Y. Lv, X. Liu, X. Wang, P. Y. Huang, D. G. Cahill, and B. Lv, *Science* **361**, 579 (2018).
 - ⁵ F. Tian, B. Song, X. Chen, N. K. Ravichandran, Y. Lv, K. Chen, S. Sullivan, J. Kim, Y. Zhou, T.-H. Liu, *et al.*, *Science* **361**, 582 (2018).
 - ⁶ T.-H. Liu, B. Song, L. Meroueh, Z. Ding, Q. Song, J. Zhou, M. Li, and G. Chen, *Physical Review B* **98**, 081203 (2018).
 - ⁷ S. Yue, F. Tian, X. Sui, M. Mohebinia, X. Wu, T. Tong, Z. Wang, B. Wu, Q. Zhang, Z. Ren, *et al.*, *Science* **377**, 433 (2022).
 - ⁸ U. Choudhry, F. Pan, X. He, B. Shaheen, T. Kim, R. Gnabasik, G. A. Gamage, H. Sun, A. Ackerman, D.-S. Yang, *et al.*, *Matter* **6**, 206 (2023).
 - ⁹ J. Buckeridge and D. O. Scanlon, *Physical Review Materials* **3**, 051601 (2019).
 - ¹⁰ S. Ku, *Journal of The Electrochemical Society* **113**, 813 (1966).
 - ¹¹ T. Chu and A. Hyslop, *Journal of The Electrochemical Society* **121**, 412 (1974).
 - ¹² S. Wang, S. F. Swingle, H. Ye, F.-R. F. Fan, A. H. Cowley, and A. J. Bard, *Journal of the American Chemical Society* **134**, 11056 (2012).
 - ¹³ J. S. Kang, M. Li, H. Wu, H. Nguyen, and Y. Hu, *Applied Physics Letters*. **115**, 122103 (2019).
 - ¹⁴ B. Song, K. Chen, K. Bushick, K. A. Mengle, F. Tian, G. A. G. U. Gamage, Z. Ren, E. Kioupakis, and G. Chen, *Applied Physics Letters* **116**, 141903 (2020).
 - ¹⁵ H. Mei, Y. Xia, Y. Zhang, Y. Wu, Y. Chen, C. Ma, M. Kong, L. Peng, H. Zhu, and H. Zhang, *Physical Chemistry Chemical Physics* **24**, 9384 (2022).
 - ¹⁶ M. van Schilfgaarde, T. Kotani, and S. Faleev, *Physical review letters* **96**, 226402 (2006).
 - ¹⁷ D. Pashov, S. Acharya, W. R. Lambrecht, J. Jackson, K. D. Belashchenko, A. Chantis, F. Jamet, and M. van Schilfgaarde, *Computer Physics Communications* **249**, 107065 (2020).
 - ¹⁸ S. Ismail-Beigi, *Journal of Physics: Condensed Matter* **29**, 385501 (2017).
 - ¹⁹ B. Cunningham, M. Gruening, D. Pashov, and M. van Schilfgaarde, “QSGW: Quasiparticle Self consistent GW with ladder diagrams in W,” (2023), preprint arXiv 2302.06325.
 - ²⁰ S. Hirata and M. Head-Gordon, *Chemical Physics Letters* **314**, 291 (1999).
 - ²¹ S. Acharya, D. Pashov, A. N. Rudenko, M. Rösner, M. van Schilfgaarde, and M. I. Katsnelson, *npj Computational Materials* **7**, 1 (2021).
 - ²² J. C. Hensel, H. Hasegawa, and M. Nakayama, *Phys. Rev.* **138**, 225 (1965), si conduction masses are 0.91 and 0.19.
 - ²³ P. Lautenschlager, M. Garriga, L. Vina, and M. Cardona, *Phys. Rev. B* **36**, 4821 (1987).
 - ²⁴ “Semiconductors · Group IV Elements, IV-IV and III-V Compounds. Part b - Electronic, Transport, Optical and Other Properties,” Copyright 1998 Springer-Verlag Berlin Heidelberg.
 - ²⁵ I. Vurgaftman, J. R. Meyer, and L. R. Ram-Mohan, *Journal of Applied Physics* **89**, 5815 (2001).
 - ²⁶ S. Acharya, D. Pashov, A. N. Rudenko, M. Rösner, M. v. Schilfgaarde, and M. I. Katsnelson, *npj 2D Materials and Applications* **6**, 33 (2022).
 - ²⁷ M. Grzeszczyk, S. Acharya, D. Pashov, Z. Chen, K. Vakinova, M. van Schilfgaarde, K. Watanabe, T. Taniguchi, K. Novoselov, M. Katsnelson, *et al.*, *Advanced Materials* , 2209513 (2023).
 - ²⁸ S. Acharya, C. Weber, D. Pashov, M. van Schilfgaarde, A. I. Lichtenstein, and M. I. Katsnelson, arXiv preprint [arXiv:2204.11081](https://arxiv.org/abs/2204.11081) (2022).
 - ²⁹ “Input and output data for reproducing the results/figures from the paper are kept at,” .